

The Onset of Spiral Structure in the Universe

Debra Meloy Elmegreen¹ and Bruce G. Elmegreen²

ABSTRACT

The onset of spiral structure in galaxies appears to occur between redshifts 1.4 and 1.8 when disks have developed a cool stellar component, rotation dominates over turbulent motions in the gas, and massive clumps become less frequent. During the transition from clumpy to spiral disks, two unusual types of spirals are found in the Hubble Ultra Deep Field that are massive, clumpy and irregular like their predecessor clumpy disks, yet spiral-like or sheared like their descendants. One type is “woolly” with massive clumpy arms all over the disk and is brighter than other disk galaxies at the same redshift, while another type has irregular multiple arms with high pitch angles, star formation knots and no inner symmetry like today’s multiple-arm galaxies. The common types of spirals seen locally are also present in a redshift range around $z \sim 1$, namely grand design with two symmetric arms, multiple arm with symmetry in the inner parts and several long, thin arms in the outer parts, and flocculent, with short, irregular and patchy arms that are mostly from star formation. Normal multiple arm galaxies are found only closer than $z \sim 0.6$ in the UDF. Grand design galaxies extend furthest to $z \sim 1.8$, presumably because interactions can drive a two-arm spiral in a disk that would otherwise have a more irregular structure. The difference between these types is understandable in terms of the usual stability parameters for gas and stars, and the ratio of the velocity dispersion to rotation speed.

Subject headings: galaxies: fundamental parameters — galaxies: photometry — galaxies: spiral — galaxies: structure

1. Introduction

Galaxies at redshifts beyond $z \sim 1$ become increasingly irregular (Abraham et al. 1996; Conselice et al. 2005; Lotz et al. 2006; Elmegreen et al. 2007; Cameron et al. 2011; Shapley

¹Vassar College, Dept. of Physics and Astronomy, Poughkeepsie, NY 12604

²IBM Research Division, T.J. Watson Research Center, Yorktown Hts., NY 10598

2011; Buitrago et al. 2013; Lee et al. 2013) as a result of rapid gas accretion (Queyrel et al. 2012), strong gravitational instabilities (Bournaud et al. 2007; Genzel et al. 2008; Ceverino et al. 2010; Wisnioski et al. 2011), and distortions produced by massive clumps (Elmegreen & Elmegreen 2005) and mergers (Kartaltepe et al. 2012; Puech et al. 2012; Kaviraj et al. 2013; McLure et al. 2013). Most of this change is driven by increasing self-gravity in the gaseous component of the disk, which increases in relative mass and Mach number toward higher redshifts (Tacconi et al. 2013; Bothwell et al. 2013). Local disks like the Milky Way have a relatively small gas fraction in the inner few scale lengths, and self-gravity operates somewhat separately in the stars and gas, making spiral arms in the stars on large scales, and molecular clouds in the gas on small scales.

Star formation processes may vary also with these morphologies, from what is presumably a collapse of gas to dense cores as a result of the strong instabilities at high redshift, to secondary instabilities inside gas that is first compressed by quasi-stable spirals or previous generations of star formation. The star formation efficiency and maximum mass of a bound stellar cluster could change too, perhaps explaining the prevalence of massive globular clusters in early phase disks (Shapiro et al. 2010; Elmegreen et al. 2012).

A number of recent surveys have extended studies of galaxy structure and evolution through much larger fields and at longer wavelengths than the original HUDF optical study, including COSMOS (Cosmic Evolution Survey; Scoville et al. (2007)) and CANDELS (Cosmic Assembly Near-Infrared Extragalactic Legacy Survey; Grogin et al. (2011)). These broad surveys provide statistical samples of galaxies and are useful for studying global galaxy properties over cosmic timescales. One of the largest recent studies includes nearly 1700 galaxies from CANDELS over the redshift range $z = 1.4 - 2.5$ to compare star formation properties and morphology based on H -band light profiles and other global indicators such as the Gini coefficient, concentration, and asymmetry (Lee et al. 2013). They conclude that the basic Hubble sequence of disk and spheroidal galaxies was set by $z \sim 2$.

We are interested in understanding the physical processes in the intermediate states of an evolving galaxy disk, between the high-redshift clumpy phase and the low-redshift spiral phase. Do the clumps gradually shrink as the turbulence dissipates and the stellar disk builds up (Cacciato et al. 2012; Elmegreen et al. 2013), or is there a new morphology with massive substructures that are both spiral-like and clump-like at intermediate redshifts?

In an unpublished study of ~ 800 spiral galaxies out to $z \sim 0.8$ in the COSMOS fields based on WFPC2 optical images, we found a mixture of grand design, multiple arm, and flocculent spirals over the whole redshift range, although the fraction of multiple arm galaxies increased at lower redshift. In a study of ~ 200 galaxies out to $z \sim 1.4$ (Elmegreen et al. 2009a) in the GEMS (Galaxy Evolution from Morphology and SEDS; Rix et al. (2004) and

Great Observatories Origins Deep Survey (GOODS Giavalisco et al. (2004)) fields, we found these three morphologies out to $z \sim 1$ and also found two clumpy types that overlapped in the same redshift range. One type had massive clumps with no evident underlying disk, and the other type had equally massive clumps with an underlying red disk. The ages and surface densities of the clumps and interclump regions suggested that the former evolved into the latter as the disks grew from dispersed clumps. Two similar types were also found at $z \sim 2$ in the UDF (Elmegreen et al. 2009b) where about half of the clumpy galaxies had red bulges that were older and more massive than the other clumps, and the other half had no bulge-like clumps. The ages of these clumps also suggested an evolutionary sequence in the characteristic morphology of spirals, although at $z \sim 2$ we could not measure the faint interclump population.

Here we focus on early-phase spirals rather than late-phase clumps. The combination of depth and resolution needed to examine spiral structure at high redshift is available only in the Hubble Ultra Deep Field (UDF; Beckwith et al. 2006) optical ACS images, so we examine morphology primarily from these images. We supplement these with the WFC3 *H*-band images of the UDF when available, although the decreased resolution and longer wavelength sometimes miss spiral details. This paper examines disk galaxies as a function of redshift out to $z \sim 4$ in the UDF, dividing the spiral types into the usual classifications of grand design (two symmetric arms), multiple arm (several long arms with an irregular distribution in the outer parts) and flocculent (small patches of star formation throughout the disk). We also look for unusual morphologies that could be transition cases between clumpy and spiral disks.

We find grand design spirals out to at least $z = 1.8$ in the UDF. The highest redshift grand design spiral so far reported is in the 3-arm galaxy BX442 at $z = 2.18$ (Law et al. 2012). At these high redshifts, the HST ACS optical bands show only the restframe ultraviolet, where star formation dominates. We should still be able to see spiral structure in the restframe UV, however. GALEX images show spiral arms in local galaxies in restframe NUV and FUV, in the familiar beads-on-a-string pattern of star formation; each string is an arm in the visible bands. Thus we can look for spirals in the higher redshift galaxies by the filamentary alignment of their star formation clumps, as well as look in the *H*-band directly for spiral arms. We present our observations in Section 2, an interpretation in Section 3, and our conclusions in Section 4.

2. Observations

2.1. Five Spiral Morphologies

We examined by eye the morphological details of the spiral galaxies in the UDF based on our catalog of 269 spirals larger than 10 pixels in diameter (Elmegreen et al. 2005). Of these, 184 are edge-on or too inclined to discern clear spiral structure, 8 are disturbed tidal interactions or mergers, 5 should probably have been classified as clump clusters, 20 have featureless disks except for a bulge, and 11 have no redshifts. The remaining 41, which have redshifts and clear spiral structure, are the ones included in the present study. Both the optical ACS images and the H -band images were used when available; about half of the 41 galaxies fell outside of the H -band field.

The galaxies are listed in Table 1, with photometric redshifts from Rafelski et al. (2009). The redshifts, which include UV data, are accurate to $\sim 0.1(1+z)$; 36 of the 41 galaxies have only one probability peak $P(z)$, which makes their redshifts relatively unambiguous. Three of the remaining four have a secondary probability peak at a redshift less than 0.1 different from the primary redshift; UDF 501 with a primary redshift of 1.37 has a secondary probability peak nearby at $z = 1.12$; UDF 9018 with a primary at $z = 1.19$ has a secondary at $z = 0.78$. The table also includes the restframe B -band absolute magnitude, the effective radius, the exponential disk scale length, the Sersic index, and the spiral arm type, to be discussed more below.

Figure 1 shows 15 spiral galaxies from the UDF in color images from the UDF Skywalker that were made from ACS archival images in bands B_{435} , V_{606} , and i_{775} (Beckwith et al. 2006). The black and white images are of the third galaxy from the left in each row, taken in H_{F160W} band with WFC3 for HUDF09 and downloaded through the HST MAST HSLP archives (Bouwens et al. 2011). The UDF numbers from Coe et al. (2006) are indicated in the upper left of each frame. White bars in the lower left of each frame indicate an angular scale of $1''$, while white bars in the upper right indicate a linear scale of 5 kpc. For reference, the pixel scale of the optical HUDF images is $0.03''$, with a FWHM resolution of $0.1''$ (Oesch et al. 2007), while the H -band HUDF09 image has a pixel scale of $0.06''$ and a FWHM resolution of $0.16''$ (Oesch et al. 2010).

Each row in Figure 1 is a different morphological type. The top row has three conventional grand design galaxies (designated type “G”) with fairly symmetric spiral arms, central bulges or bars, and smooth underlying disks. The arms are open, wrapped at most 180° , and dotted with star formation knots and streaks. Other grand design galaxies are in Table 1. The largest redshift for this morphology in the UDF is $z = 1.8$ for UDF 9444.

In the second row are three normal-looking multiple arm galaxies (type “M”) that resemble a common type in the local universe. The arms in the outer parts are long and thin, sometimes wrapping for 180° or more, and the arms in the inner parts are usually symmetric, sometimes with a short bar. The highest redshift that we found for this type of spiral is 0.6 for UDF 2607 in the figure. This is significantly smaller than the largest redshift for the grand design spirals, of which there are four with $z > 1$. Thin arms in multiple arm galaxies like this require cool disks. It may be that this cool phase comes later than the first grand design galaxies, whose structure may be induced by strong bars or interactions even in hot disks (see below).

The third and fourth rows contain galaxy morphologies that are relatively uncommon in the local universe. In the third row are multiple arm galaxies with long, thick and bright arms that cover most of the disks. The arms are clumpy and the clumps are relatively large. There are bright interarm clumps too. Galaxies 968 and 5417 have offset nuclei. Local analogs also including a high proportion with offset nuclei are types Ic in the Kiso Ultraviolet Survey of Galaxies (Miyuchi-Isobe, Maehara, & Nakajima 2010), whose clumps were found to be comparable in mass to the clumps in UDF clumpy galaxies (not shown in the figures here), and which also have multiple spiral arms (Elmegreen et al. 2013). The row-three galaxies in Figure 1 differ from the Kiso type Ic galaxies, however, because the row-three galaxies have arms that are relatively thick, bright and nearly continuously filled with clumps. We consider this a new morphology for spiral galaxies that should be placed between purely clumpy galaxies at high redshift and density-wave spiral galaxies at low redshift. Their distinctive feature is their thick patchy long arms. A term that comes to mind is “woolly” (type “W” in what follows) which is somewhat like “flocculent” but connotes something more dense in structure. Three more of these galaxies are shown in the top of Figure 2.

The fourth row in Figure 1 shows another odd type of structure consisting of long, generally thin and multiple arms with haphazard distributions and varying pitch angles. There are bright star-formation knots along the arms, which is a common feature of most spiral arms, but no symmetry. Some have small bars which seem unrelated to the spirals. This is another morphology that one might expect in an era of strong gravitational instabilities, which readily produce large, shearing and chaotic-looking material arms, but the clump size has decreased by now, perhaps because of a reduced turbulent speed in the interstellar gas. Six more examples of this class are in Figure 2. We refer to this type descriptively again, calling them “irregular long” arm galaxies (type “IL”). That is, they are not like classical irregulars which tend to have no spiral arms, nor are they like grand design or multiple arm galaxies, which tend to have at least a little symmetry, especially in the center. To distinguish this class from those in the second row, we sometimes call the latter “normal” multiple arm galaxies in what follows.

The fifth row in Figure 1 shows common looking flocculent galaxies (type “F”) with small patches of star formation and faint traces of underlying spiral waves in the stars. Often the pitch angles are high, making the arms look nearly radial (UDF 2525 in the figure, or UDF 9204, not shown). In the presence of shear, such high pitch angles correspond to young ages, and that youth is consistent with the patches being mostly star formation regions. In a flocculent galaxy, most of the structure is from star formation and presumably, therefore, instabilities in the gas.

To consider what effects might be caused by resolution limitations at different redshifts, we note that in a Λ CDM cosmology (Spergel et al. 2003), the angular size of a 10 kpc disk is a constant $\sim 1.4''$ between redshifts 0.6 and 4, which applies to 15 of the 24 galaxies in Figures 1 and 2. A glance at Table 1 reveals that there are galaxies of all 5 spiral types across this redshift range, which implies that angular resolution is not systematically varying among the different types. For example, UDF 2607 and 7556, two normal multiple arm galaxies in Figure 1, have redshifts of 0.60 and 0.53, respectively; UDF 968 and 3372, two woollies, have the same redshifts of 0.50 and 0.78. UDF 2525, a flocculent galaxy, has a redshift of 0.63, and UDF 9253 (not shown) is a grand design galaxy at a redshift of 0.52. Thus, their different morphologies are not an artifact of different resolutions or different restframe wavelengths. Further discussions of resolution and bandshifting effects are described in Elmegreen et al. (2009a) regarding GEMS and GOODS morphology.

Following the method in Elmegreen et al. (2009a), we Gaussian-blur two of the present galaxies (“M” types UDF 423 at $z = 0.29$ and UDF 7556 at $z = 0.53$) to the resolution of a third (“W” type UDF 5417 at $z = 1.11$), and also re-pixelate the closest of these (UDF 423) to approximately match the pixel scales of the other two. We start with the z_{850} image of UDF 5417, the V_{606} image of UDF 7556, and the B_{435} image of UDF 423; these correspond to similar restframe wavelengths of ~ 400 -340 nm. The pixel scales are the same for each pass band and the FWHMs of stars are similar: 3.12, 2.88, and 3.25, respectively. At the distances to these galaxies, 1 px corresponds to 247 pc, 188 pc, and 129 pc, respectively. Thus the FWHM in UDF 5417 corresponds to 770 pc, which is 4.1 px in UDF 7556 and 5.9 px in UDF 423. We match the scale of the most distant galaxy by blurring the closer galaxies by an amount equal to $[(\text{px in } 770\text{pc})^2 - (\text{px in FWHM})^2]^{1/2}$ and dividing that by $(8 \ln 2)^{1/2}$ to get the Gaussian dispersion. These give Gaussian blur dispersions of 1.22 px for UDF 7556 and 2.12 px for UDF 423. For the latter we also block-average 2×2 pixels to approximate the linear resolution of the distant galaxy, UDF 5417.

The results of the Gaussian blurs are shown in Figure 3, where each galaxy is presented with approximately the same linear scale, pixel scale, and restframe wavelength, as mentioned above. Evidently, the overall appearances of the nearby multiple-arm galaxies (UDF 7556

and UDF 423) are not substantially changed when the galaxies are blurred to look like the distant, woolly spiral (UDF 5417). Bandshifting and resolution effects are not significant. The woolly galaxy has bright irregular arms and large interarm star formation patches, giving it a high surface brightness. This surface brightness is larger still, when compared to the other two galaxies, if we consider that we have not corrected for cosmological surface brightness dimming in Figure 3: that would make the blurred galaxies dimmer in proportion to $(1+z)^{-4}$, which means a factor of 0.28 and 0.14 for UDF 7556 and UDF 423, respectively. Such a reduction in surface brightness would make the two multiple arm galaxies barely visible in this figure if we were to include it.

2.2. Properties of the Five Morphologies

Figure 4 shows the redshift dependence of the restframe B -band absolute magnitudes of the UDF spiral galaxies in Figures 1 and 2 and Table 1. It also shows the surface brightnesses measured on a relative scale as $10^{-0.4M_B}/R_{\text{eff}}^2$ for R_{eff} the effective radius in Table 1, in kpc. The restframe B absolute magnitudes come from COMBO17 (Classifying Objects by Medium-Band Observations, a spectrophotometric 17-filter survey by Wolf et al. 2003), but have been modified using an interpolation between U , B , and V bands to account for our use of Rafelski et al. (2009) redshifts instead of COMBO17 redshifts. The effective radii come from GALFIT in a previous paper based on restframe B band (Elmegreen et al. 2007) and were also adjusted to the Rafelski et al. (2009) redshifts since the measurements originally used redshifts from Coe et al. (2006).

The overall brightness of our sample in absolute magnitudes increases with redshift, partly as a selection effect for identifying these objects and partly following the general increase in the universal star formation rate. The surface brightness is more constant, suggesting an increase in R_{eff} with restframe luminosity. The woolly UDF spirals (green x-marks) and those with normal multiple arms (blue triangles) are intrinsically brighter than the others, on average, for all redshifts. The flocculents are fainter (as they are locally). All types but the normal multiple arm galaxies span the full range of redshifts, out to $z \sim 1.4$ in most cases, and $z = 1.8$ for one grand design galaxy. We find no spiral galaxies of any type beyond this redshift, even indirectly in the form of a spiral-like alignment of star formation clumps, nor does the H -band image reveal spirals unnoticed in optical bands.

We measured the three largest star-forming clumps in several woolly and normal multiple arm galaxies. For the normal multiple-arm galaxies, the three largest clumps contribute 0.5% to 2% of the flux in the observer i_{775} band and 3% to 5% of the flux in the B_{435} band. For the woolly galaxies, the three largest clumps contribute 5% to 15% of the i_{775} band flux, and

10% to 25% of the B_{435} band flux. Thus the largest clumps are ~ 10 times more luminous in the woolly galaxies than in the normal multiple-arm galaxies.

We also compared the arm-interarm contrasts in the UDF grand design galaxies with those in local grand design galaxies, as measured from azimuthal profiles. UDF 2 is shown along with local grand design spiral NGC 3031 (Elmegreen & Elmegreen 1984) in Figure 5. The arm-interarm contrasts are about same in the UDF as in the local grand designs, with the arms 1 to 2 mag arcsec $^{-2}$ brighter than the interarms in the restframe V band.

The Sersic indices n from Elmegreen et al. (2007) GALFIT measurements of the rest-frame B images are shown in Figure 6 as a function of spiral morphology. Because the galaxies in the present study are all disk galaxies, the indices average around 1 for exponential disks. The outliers with large n in the figure have large central bulges. The woolly types stand out as having low n , which is consistent with their distributed light consisting of bright arms and interarm clumps throughout the disk. This low- n value for woollies is similar to what was found for the most clumpy galaxies in the UDF (Elmegreen et al. 2007), further suggesting that the woollies are an intermediate type between clumpy galaxies at high redshift and normal spiral arm galaxies at low redshift.

3. Interpretation

The five spiral morphologies discussed in the previous section correspond to theoretical expectations based on the variation of several key parameters, such as Q_{gas} , Q_{star} , and $L_{\text{Jeans}}/R_{\text{gal}}$, which are the Toomre Q values for gas and stars, and the ratio of the gaseous Jeans length to the galaxy size (which is proportional to the square of the ratio of the gas velocity dispersion to the rotation speed). The presence of strong interactions and bars is a fourth determinant of structure. In addition, recent observations of gas kinematics have shed light on how disk structures evolve with redshift. Molecular gas observations by Tacconi et al. (2010, 2013) revealed that massive star-forming galaxies have progressively higher gas fractions at $z \sim 1.2$ and $z \sim 2.3$ compared with the present. $\text{H}\alpha$ studies by Reddy et al. (2006) and Erb et al. (2006, 2009) show higher star formation rates in high redshift galaxies, with more massive galaxies reaching their peak star formation first. Kinematic studies by Förster Schreiber et al. (2009) and Genzel et al. (2011) showed that massive clumpy galaxies at $z \sim 2$ have high velocity dispersions, and Kassin et al. (2007) and Wright et al. (2009) showed that velocity dispersion decreases with decreasing redshift. These gas fractions and kinematics are consistent with numerical simulations (Bournaud et al. 2007; Bournaud & Elmegreen 2009; Bournaud et al. 2013) showing more massive clumps in the early Universe than at present. Although the observations do not yet extend to the five different spiral types

studied here, with these parameters in mind, we can reconstruct or predict what should be happening in their disks.

First of all, grand design galaxies should have relatively low Q_{star} so the stellar disk is only marginally stable and readily forms strong stellar spiral arms following perturbations from bars and companions. Gravitational instabilities in the gas, involving Q_{gas} , are not particularly important for the overall grand design structure, and star formation itself is secondary, following independent gravitational instabilities in the spiral-shocked gas and other compressed gas. Normal multiple-arm galaxies (the second row in Fig. 1) should also have relatively low Q_{star} , although perhaps in some cases not as low as in a strong grand-design galaxy, but the multiple arm types tend to lack strong symmetric forcing, i.e., strong bars and interactions. In both cases, stellar gravity is relatively strong, reflecting a high ratio of disk mass to halo mass in the optical parts.

Flocculent galaxies (row 5 in Figure 1) should have relatively weak stellar gravity in the disk so that stellar spiral arms tend to be absent or weak. This weakness corresponds to a somewhat higher Q_{star} and azimuthal parameter J (Lau & Bertin 1978) (or lower X ; Julian & Toomre 1966), and to a relatively small disk-to-halo mass ratio. A difference between grand design and flocculent galaxies with respect to the disk-to-halo ratio was measured in Elmegreen & Elmegreen (1990) using outer HI rotation curves. A hot stellar disk, or a relatively large mass in the thick disk, can make a galaxy flocculent in the absence of strong bars or companion perturbations. Flocculent galaxies tend to be fainter than grand design galaxies (Elmegreen & Elmegreen 1987), consistent with the luminosity class introduced by van den Bergh (1960). This faintness is also evident from Figure 3.

The two new types, the “woolly” and “irregular long” arm galaxies, also fit into this three-parameter scenario. The woollies should be strongly gravitationally unstable in both the stars and the gas (Q_{star} and Q_{gas} relatively small) so spirals readily form even without bars or companion perturbations, and stars form nearly everywhere in the spiral-compressed gas. The clumps are large so $L_{\text{Jeans}}/R_{\text{gal}}$ is large, presumably because the velocity dispersion is relatively high compared to the rotation speed – high meaning several tens of percent, almost like what is observed in clumpy galaxies (Förster Schreiber et al. 2009). There should also be a significant mass of stars in the disk, however, unlike the pure clumpies, and perhaps a thick disk or spheroid as well, causing the disk instabilities to make spirals rather than clumps (Bournaud & Elmegreen 2009). Irregular long-arm galaxies should also have strong disk instabilities (Q_{star} and Q_{gas} relatively small) but now $L_{\text{Jeans}}/R_{\text{gal}}$ is small too (making the clumps small), presumably because the gaseous velocity dispersion has decreased.

The structure of these intermediate spiral types resembles that in the later stages of clumpy-disk simulations by Bournaud et al. (2013). Galaxies 968 and 1971 in Figure 1

were also shown in Figure 15 of that paper. According to the simulations, the transition from clumpy structure to spiral structure takes about 1 Gyr, and the irregular long-arm structure occurs at a time between 500 and 800 Myr after the galaxy forms. The gas in the simulations has a high velocity dispersion of $\sim 40\text{--}50\text{ km s}^{-1}$ and is gravitational unstable to star formation, with $Q \sim 1$. At later stages, $z \sim 1$ or less, massive clumps become relatively rare, disks begin to settle down, and rotation begins to dominate over turbulent motions in the gas (Genzel et al. 2006; Kassin et al. 2007; Förster Schreiber et al. 2009). Bars appear at about the same time (Sheth et al. 2012).

Considering the basic parameters that determine galactic structure, the disk morphologies that have been identified at intermediate to high redshifts might be placed into the following sequence for the development of spiral structure in galaxies over time. The first stage is when the disk is nearly pure clumps and there is relatively little interclump emission from older stars (Elmegreen et al. 2009a,b). This corresponds to a gas-dominant phase when interstellar turbulent speeds are also high (Bournaud et al. 2007). The second stage is clumpy but with an interclump stellar population (Elmegreen et al. 2009a), presumably resulting from the dissolution of clumps. A classical bulge and thick disk form in these first two stages. In subsequent stages, there are enough hot stars from the earlier stages (in a thick disk and spheroid) that gravitational instabilities make spirals rather than clumps (Bournaud & Elmegreen 2009). At first, there may still be a relatively high gas fraction and turbulent speed, making the morphology we identify here as “woolly,” namely with long and thick arms covered with giant star forming regions. Then, as the gas cools and additional gas accretes more slowly, the star-forming clumps get smaller even if the disk stays highly unstable, forming spirals all over in an irregular way. This is the irregular long-arm phase highlighted here. Finally the stellar instabilities calm down as the stellar disk warms up (Cacciato et al. 2012), and the gas cools as it accretes at a slower rate without the irregular forcing that formerly drove fast turbulence. Gaseous instabilities also become weaker at these later phases, when the gas fraction drops, and this, in addition to a decreasing star formation rate, also limits the turbulent speed. Then normal multiple arm and flocculent galaxies appear. Bars and strong interactions should make grand design spirals in the main disks of the latter stages, but not in the pure-clump phases, which have too few disk stars and disk stars that are too hot to organize into a coherent spiral pattern. Presumably, tidal arms in the outer regions of any of these galaxy types can be made by strong enough interactions (e.g. Law et al. 2012).

4. Conclusions

Spiral structure appears in the Hubble Ultra Deep Field by $z \sim 1.8$ and most prominently below $z \sim 1.4$. The observations of different spiral types are consistent with the interpretation that clumpy disks form first and then transition to spirals as the accretion rate and gas velocity dispersion decrease, and the growing population of old fast-moving stars begins to dominate the disk mass. These trends are consistent with kinematic observations and numerical simulations. Grand design structures appear somewhat earlier than the other spiral types in our survey, perhaps because strong interactions can make symmetric tidal arms with grand design structure in a disk that would otherwise have no visible spirals.

We are grateful to the referee for helpful comments.

REFERENCES

- Abraham, R., van den Bergh, S., Glazebrook, K., Ellis, R., Santiago, B., Surma, P., & Griffiths, R. 1996, *ApJS*, 107, 1
- Beckwith, S.V.W., et al. 2006, *AJ*, 132, 1729
- Bothwell, M. S., Smail, I., Chapman, S.C., Genzel, R. et al. 2013, *MNRAS*, 429, 3027
- Bournaud, F., Elmegreen, B.G., & Elmegreen, D.M. 2007, *ApJ*, 670, 237
- Bournaud, F., & Elmegreen, B.G. 2009, *ApJ*, 694, L158
- Bournaud, F., et al. 2013, *ApJ*, in press [arXiv:1307.7136]
- Bouwens, R.J. et al. 2011, *ApJ*, 737, 90S.
- Buitrago, F., Trujillo, I., Conselice, C.J., & Häussler, B. 2013, *MNRAS*, 428, 1460
- Cacciato, M., Dekel, A., & Genel, S. 2012, *MNRAS*, 421, 818
- Cameron, E., Carollo, C. M., Oesch, P. A., Bouwens, R.J., Illingworth, G.D., Trenti, M., Labbé, I., & Magee, D. 2011, *ApJ*, 743, 146
- Ceverino, D., Dekel, A., Bournaud, F. 2010, *MNRAS*, 404, 2151
- Coe, D., Benítez, N., Sanchez, F., Jee, M., Bouwens, R., & Ford, H. 2006, *AJ*, 132, 926
- Conselice, C. J., Blackburne, J. A., Papovich, C. 2005, *ApJ*, 620, 564

- Elmegreen, D.M., & Elmegreen, B.G. 1984, ApJS, 54, 127
- Elmegreen, D.M., & Elmegreen, B.G. 1987, ApJ, 314, 3
- Elmegreen, D.M. & Elmegreen, B.G. 1990, ApJ, 364, 412
- Elmegreen, B.G., & Elmegreen, D.M. 2005, ApJ, 627, 632
- Elmegreen, D.M., Elmegreen, B.G., Rubin, D.S., & Schaffer, M. 2005, ApJ, 631, 85
- Elmegreen, D.M., Elmegreen, B. G., Ravindranath, S., & Coe, D.A. 2007, ApJ, 658, 763
- Elmegreen, D.M., Elmegreen, B.G., Marcus, M., Shahinyan, K., Yau, M., & Petersen, M. 2009a, ApJ, 701, 306
- Elmegreen, D.M., Elmegreen, D.M., Fernandez, M.X., & Lemonias, J.J. 2009b, ApJ, 692, 12
- Elmegreen, B.G., Malhotra, S., & Rhoads, J. 2012, ApJ, 757, 9
- Elmegreen, B.G., Elmegreen, D.M., Sánchez Almeida, J., Muñoz-Tuñón, C., Dewberry, J., Putko, J., Teich, Y., & Popinchalk, M. 2013, ApJ, 2013, ApJ, 774, 86
- Erb, D. et al. 2006, ApJ, 646, 107
- Erb, D. et al. 2006, ApJ, 647, 128
- Förster Schreiber N. M. et al., 2009, ApJ, 706, 1364
- Genzel R. et al., 2006, Nature, 442, 786
- Genzel R. et al., 2008, ApJ, 687, 59
- Genzel R. et al., 2011, ApJ, 733, 101
- Giavalisco, M., Ferguson, H. C., Koekemoer, A.M., Dickinson, M. et al. 2004, ApJ, 600, L93
- Grogin, N.A., et al. 2011, ApJS, 197, 35
- Julian, W. H., & Toomre, A. 1966, ApJ, 146, 810
- Kartaltepe, J.S., Dickinson, M., Alexander, D.M., Bell, E.F., et al. 2012, ApJ, 757, 23
- Kassin, S.A., Weiner, B.J., Faber, S.M., Koo, D.C., et al. 2007, ApJ, 660, L35
- Kaviraj, S., Cohen, S., Windhorst, R.A., Silk, J., O’Connell, R.W., Dopita, M. A., Dekel, A., Hathi, N. P., Straughn, A., & Rutkowski, M. 2013, MNRAS, 429, L40

- Lau, Y.Y., & Bertin, G. 1978, ApJ, 226, 508
- Law, D.R., Shapley, A.E., Steidel, C.C., Reddy, N.A., Christensen, C.R., & Erb, D.K. 2012, Nature, 487, 338
- Lee, B. et al. 2013, ApJ, 774, 47
- Lotz, J. M., Madau, P., Giavalisco, M., Primack, J., & Ferguson, H. 2006, ApJ, 636, 592
- McLure, R. J., Pearce, H. J., Dunlop, J. S., et al. 2013, MNRAS, 428, 1088
- Miyauchi-Isobe, N., Maehara, H., & Nakajima, K. 2010, Pub.Nat.Astro.Ob.Japan, 13, 9
- Oesch, P.A. et al. 2007, ApJ, 671, 1212
- Oesch, P.A. et al. 2010, ApJL, 709, L16
- Puech, M., Hammer, F., Hopkins, P. F., Athanassoula, E., Flores, H., Rodrigues, M., Wang, J. L., & Yang, Y. B. 2012, ApJ, 753, 128
- Queyrel, J., Contini, T., Kissler-Patig, M., et al. 2012, A&A, 539, A93
- Rafelski, M., Wolfe, A.M., Cooke, J., Chen, H.-W., Armandroff, T.E., & Wirth, G.D. 2009, ApJ, 703, 2033
- Reddy, N. et al. 2006, ApJ, 644, 792
- Rix, H.-W., Barden, M., Beckwith, S.V.W., Bell, E.F. et al. 2004, ApJS, 152, 163
- Scoville, N. et al. 2007. ApJS, 172, 1
- Shapiro, K.L., Genzel, R., & Förster Schreiber, N.M. 2010, MNRAS, 403, L36
- Shapley, A.E. 2011, ARA&A, 49, 525
- Sheth, K., Melbourne, J., Elmegreen, D.M., Elmegreen, B.G., Athanassoula, E., Abraham, R.G., & Weiner, B.J. 2012, ApJ, 758, 136
- Spergel, D.N., et al. 2003, ApJS, 148, 175
- Tacconi, L. J., et al. 2010, Nature, 463, 781
- Tacconi, L. J., Neri, R., Genzel, R., et al. 2013, ApJ, 768, 74
- van den Bergh, S. 1960, ApJ, 131, 215

Wisnioski, E., Glazebrook, K., Blake, C., et al. 2011, MNRAS, 417, 2601

Wolf, C., Meisenheimer, K., Rix, H.-W., Borch, A., Dye, S., & Kleinheinrich, M. 2003, A&A, 401, 73

Wright, S. et al. 2009, ApJ, 699, 421

Table 1. Galaxy properties

UDF	z^a	M_B (mag) ^b	R_{eff} (kpc) ^c	Disk Scalelength (kpc) ^c	Sersic n^c	type ^d
Figure 1						
656	1.24	-18.21	3.0	1.4	3.3	G
2	0.92	-19.95	8.9	3.0	1.6	G
6188	1.03	-18.68	5.9	2.5	1.8	G
423	0.29	-21.45	8.8	3.4	1.5	M
2607	0.60	-20.55	8.5	3.2	2.1	M
7556	0.53	-20.96	3.6	2.1	1.2	M
968	0.50	-20.60	5.7	2.1	0.9	W
3372	0.78	-20.78	5.8	3.3	0.3	W
5417	1.11	-21.01	6.4	2.2	0.8	W
3268	0.25	-17.81	3.1	1.5	1.3	IL
1971	0.03	-18.54	1.4	0.6	1.7	IL
6974	0.50	-19.21	4.5	2.0	0.6	IL
7495	0.12	-14.87	1.5	1.1	0.6	F
2525	0.63	-18.81	1.8	1.4	1.7	F
501	1.37	-19.42	7.4	3.8	1.5	F
Figure 2						
9125	1.32	-20.11	5.9	2.9	0.6	W
5805	1.41	-20.07	4.6	1.6	0.4	W
4438	0.78	-20.64	6.3	6.8	0.4	W
9183	0.95	-18.38	3.0	1.9	0.8	IL
4394	0.51	-20.33	6.2	4.0	0.9	IL
8275	0.69	-20.45	11.0	3.1	1.7	IL
9455	0.47	-18.86	8.8	2.6	2.5	IL
7036	1.40	-19.26	5.1	2.4	3.6	IL
7688	2.58	-16.83	9.7	7.0	1.0	IL
Others						
8261	1.36	-19.55	4.6	2.8	1.2	G
9444	1.82	-19.24	3.2	2.4	1.3	G
9253	0.52	-21.08	6.4	3.0	1.6	G
3492	0.20	-19.65	5.4	3.8	1.0	G
4929	0.45	-19.47	1.6	1.2	1.6	G
6082	0.23	-16.72	2.3	0.8	0.4	G
328	0.24	-19.73	8.9	3.8	1.9	M
3822	0.18	-19.17	3.6	1.8	1.5	M
7112	1.12	-19.28	2.9	1.0	0.4	W
8049	0.20	-19.92	9.7	1.3	5.2	W
6862	0.51	-19.61	4.4	2.0	1.8	IL
6997	0.63	-17.02	2.9	2.0	1.0	IL
9018	1.19	-19.62	3.3	2.4	0.9	IL
1905	0.58	-17.48	2.9	1.5	1.1	F
5922	1.02	-18.32	4.1	3.4	1.2	F
9341	1.04	-18.17	3.4	2.3	1.0	F
9895	0.97	-18.65	5.7	3.6	1.1	F

^afrom Rafelski et al. (2009) except for UDF 328, which uses the COMBO17 redshift

^bfrom COMBO17, corrected to redshifts from Rafelski et al. (2009)

^cfrom Elmegreen et al. (2007), corrected to redshifts from Rafelski et al. (2009)

^d“G” = grand design (two prominent and symmetric arms), “M” = normal multiple arms, usually symmetric and 2-arm in the inner parts, “W” = “woolly” in reference to thick and patchy long arms, “IL” = “irregular long” arms, as distinct from multiple arms because there is little symmetry, “F” = flocculent with faint patchy and short arms.

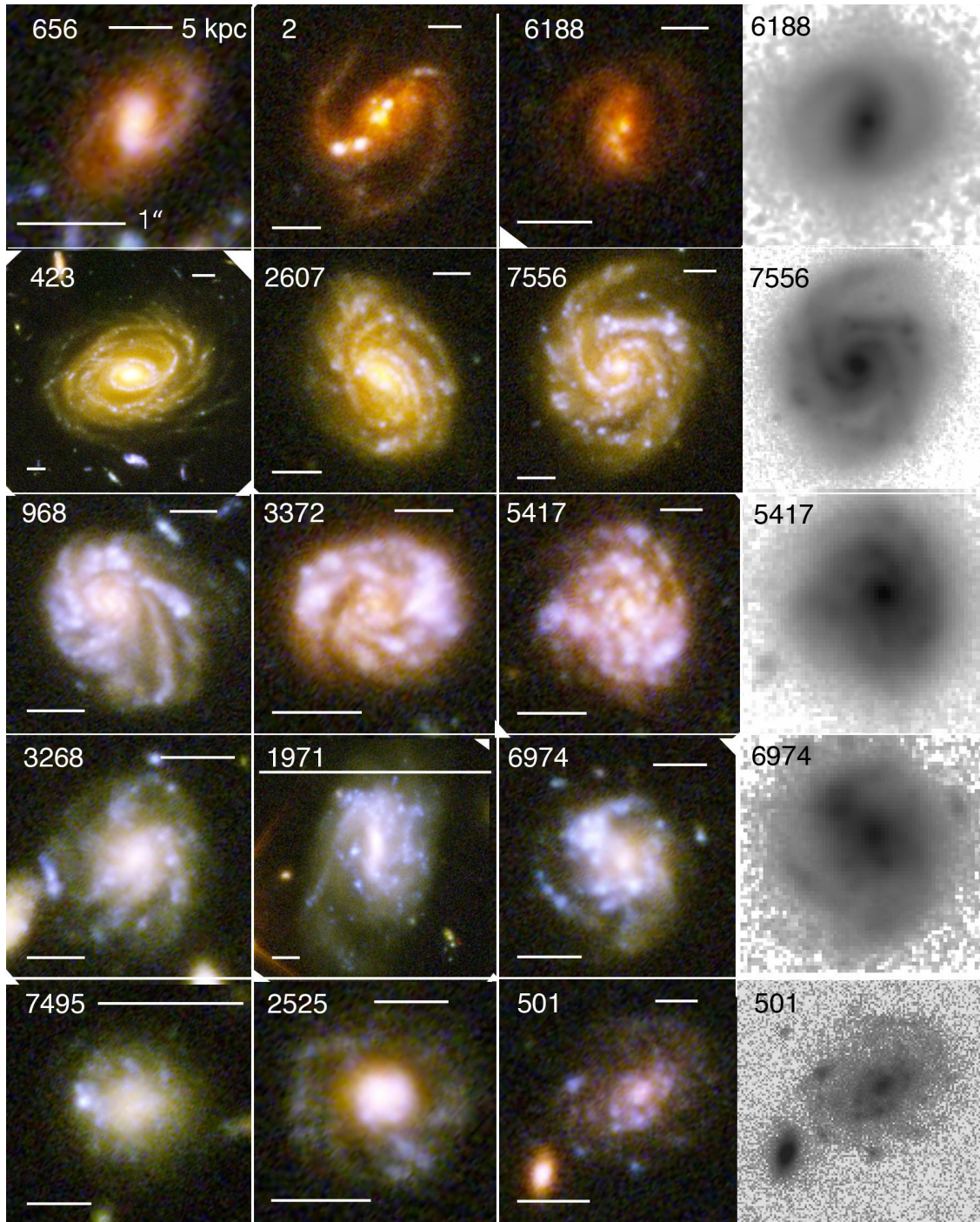


Fig. 1.— Five spiral arm morphologies in the UDF with three examples of each (in color) and an H-band image of the right-most example in black and white. In each image, the bar on the lower left indicates an angular scale of $1''$, while the bar on the upper right indicates a linear scale of 5 kpc. From top to bottom, the morphologies are: grand design, normal multiple arm, woolly, irregular long-arm, and flocculent. The properties of these galaxies are in Table 1. What we call woolly consists of thick, patchy and long arms, in contrast to flocculent galaxies which have numerous short and patchy arms. The irregular long-arm type consists of numerous thin arms with bright beads of star formation in them and an overall irregular or asymmetric structure.

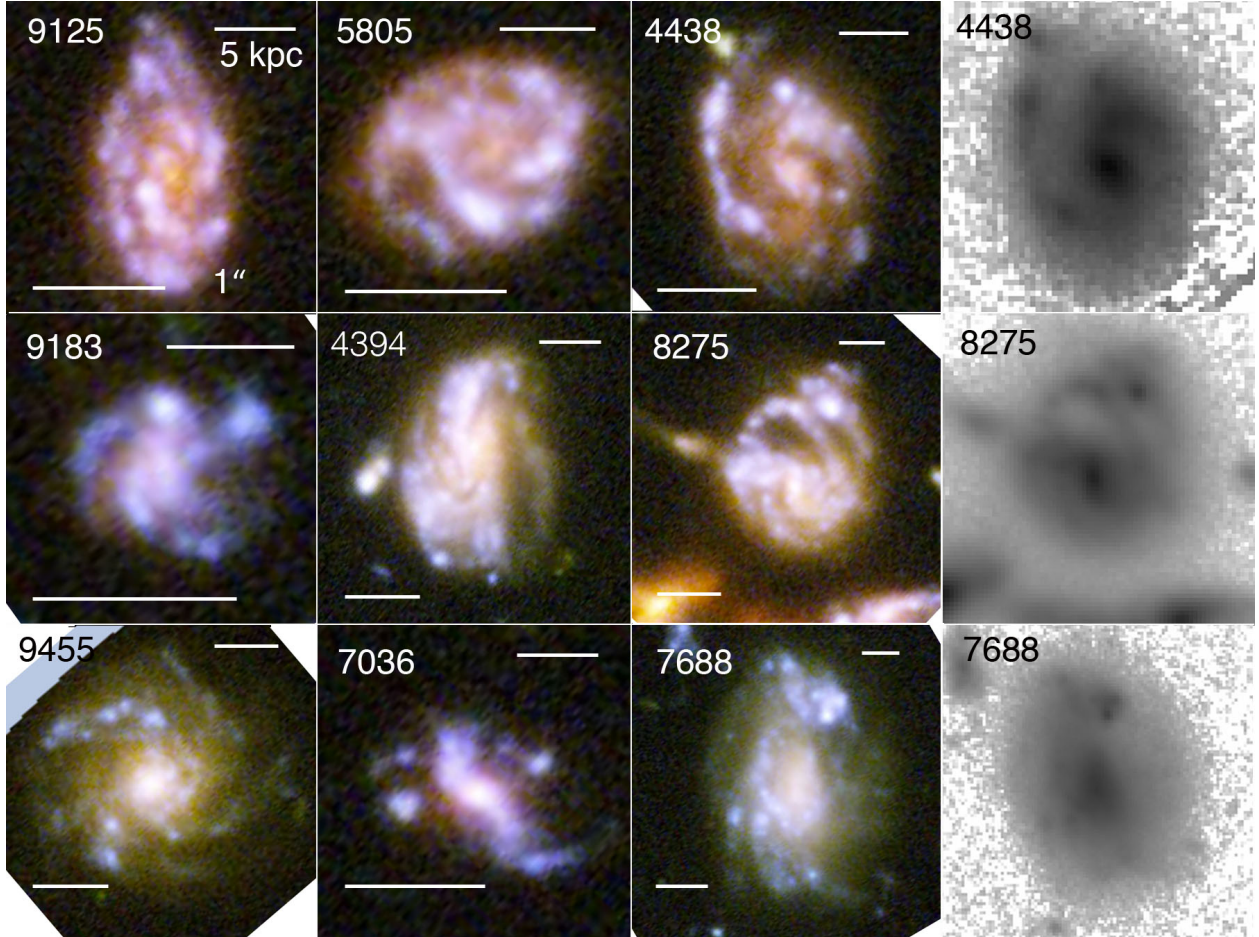


Fig. 2.— Additional examples of the two new morphologies discussed here. The top row contains more woolly galaxies and the bottom two rows contain more irregular long-arm galaxies. Scales are for $1''$ and 5 kpc, as in Figure 1.

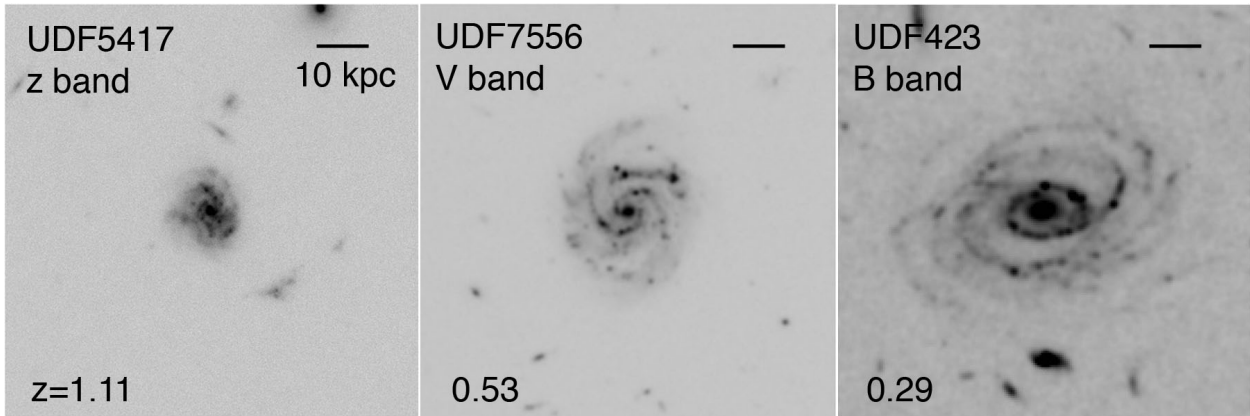


Fig. 3.— UDF 5417 is a woolly galaxy; the other two are multiple arm, and have been Gauss-blurred to match the resolution of the woolly. The different bands all correspond to restframe ~ 400 nm. The black line indicates a linear scale of 10 kpc.

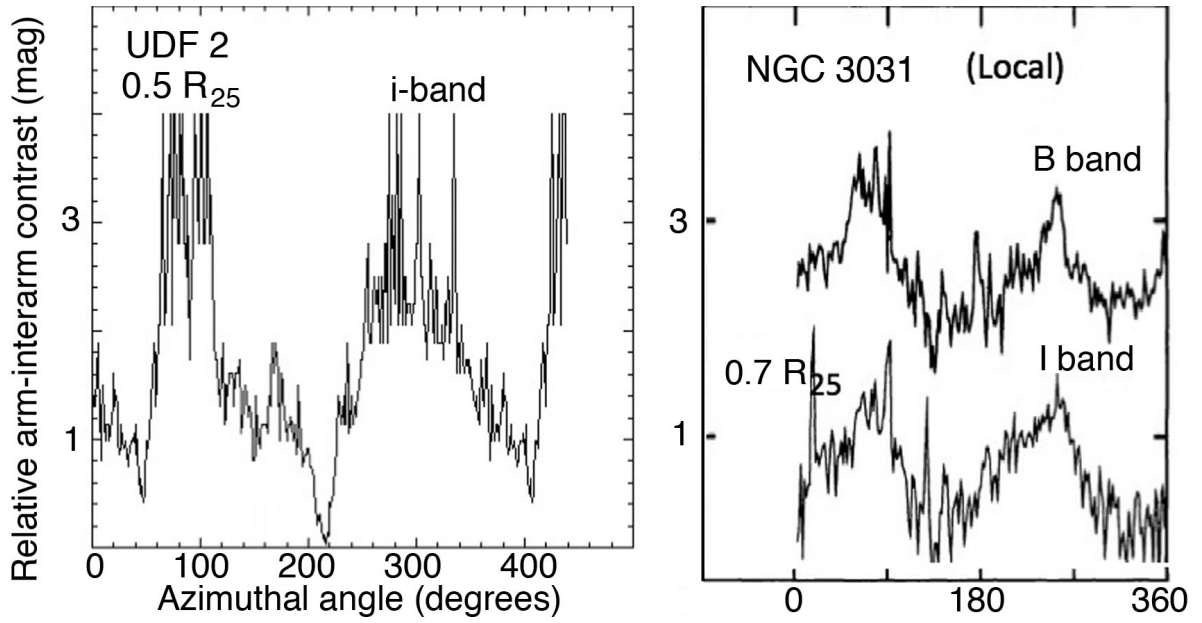


Fig. 5.— Arm-interarm contrasts are shown for the grand design galaxies UDF 2 and local NGC 3031.

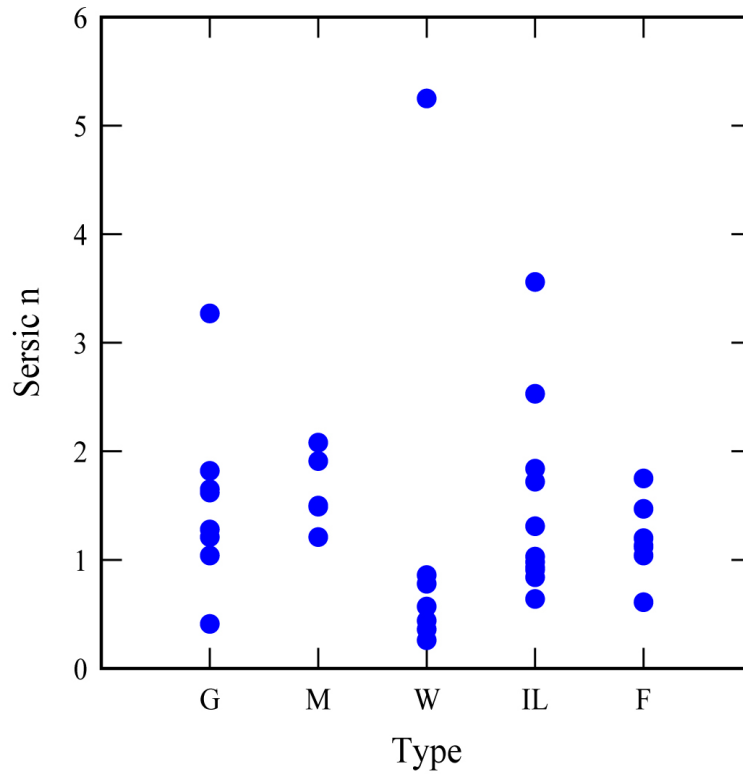


Fig. 6.— Sersic index n as a function of spiral morphological type. The woolly spirals have systematically low n , consistent with their having big clumps spread throughout the disk to give flatter light profiles. The outliers with high n have large central bulges.